J. Fluid Mech. (1987), *vol.* 175, *pp.* 537–555
Printed in Great Britain

An experimental study of the steady and unsteady flow characteristics of stirred reactors

By M. YIANNESKIS,
Kings College London, Mechanical Engineering Department, Strand, London WC2R2LS, UK

Z. POPIOLEK
Instytut Ogrzewnictwa, Wentylacji, i Ochrony Powietrza, Politechnika Slaska, 44-101 Gliwice, Poland

AND J. H. WHITELAW
Fluids Section, Mechanical Engineering Department, Imperial College of Science and Technology, Exhibition Road, London SW7 2BK, UK

(Received 24 October 1984 and in revised form 15 July 1986)

Liquid flow in a baffled stirred reactor vessel driven by a six-blade disk impeller has been investigated experimentally. Laser-slit photography provided an overview of the flows which were quantified by measurements of velocity characteristics, obtained with a laser-Doppler anemometer, for an impeller rotational speed of 300 r.p.m. and for three impeller clearances from the bottom of the vessel. The mean flow results show an inclination of the impeller stream and the formation of ring vortices above and below the impeller, which depend on the clearance; the flow was strongly three-dimensional with large regions having circumferential velocities in a direction opposite to that of the impeller rotation. Impeller-induced torque measurements show that the Power number is invariant with clearance for turbulent-flow Reynolds numbers ($\geqslant 40000$) and increases with impeller diameter. The flow structure was controlled mainly by convection and pressure forces with turbulent mixing important in the impeller region.

1. Introduction

Considerable attention has been devoted to the study of the flow processes in stirred reactors and stems from their frequent use in engineering practice. The fluid contained in a stirred vessel is circulated by a rotating impeller with baffles positioned along the periphery of the vessel to inhibit the free surface vortex and to increase small-scale mixing. The flow around a blade of a disk-type impeller interacts with the rotating flat blade to generate circulations in the circumferential and radial directions respectively which, in turn, give rise to three-dimensional roll vortices behind each blade.

The mean flow in stirred reactors can be characterized by power requirements which have been considered, for example, by Uhl & Gray (1966) and by the velocity and turbulence properties examined, for example, by Cutter (1966), Mujumdar *et al.* (1970), Günkel & Weber (1975), and others. These investigations of the flow have made use of photographic techniques and/or Pitot, hot-wire and hot-film probes and show that two ring vortices usually exist with one above and one below the impeller. The influence of the periodicity introduced by the blades of the impeller decreases

with distance from the impeller tip but details of the flow in the vicinity of the impeller are largely unknown. Laser-Doppler velocimetry is well suited for investigations of a flow of a highly vortical nature and was employed by Reed, Princz & Hartland (1977) and van der Molen & van Maanen (1978), to provide a description of the flow in the impeller region.

The flow processes associated with the trailing vortex region are of interest and van't Riet & Smith (1973, 1975) recorded the flow of tracer particles in a stirred vessel with video, fixed still and cine cameras rotating synchronously with the agitator. The visualization showed that the vortices behind the blades maintained their identity for two to three blade lengths and that the vortex axis was very nearly horizontal with position independent of speed for Reynolds numbers above 5000. Van't Reit, Bruijn & Smith (1976) examined the impeller flow with a stationary hot-film probe and observed that the vortices were broken up at the baffles and the vessel walls. Van der Molen & van Maanen (1978) drew similar conclusions and reported that the circulation velocity in the vortices is dependent on the impeller geometry and in particular on the blade thickness.

The present work was prompted by the need for quantitative information of the vortex structure and of the influence of geometrical variables. It is concerned with the single-phase, isothermal turbulent flow in a baffled vessel caused by a six-bladed disk impeller rotating at 300 r.p.m. Flow visualization and impeller-induced torque measurements were made to determine the effect of impeller size and clearance on the flow and laser-Doppler anemometry was used to measure the mean flow and turbulence fields for three values of impeller clearance which the visualization had suggested to be important. The present investigation provides a detailed and accurate quantitative description of the flow processes in all parts of a vessel of geometry representative of current practice with a free surface and realistic impeller arrangement. The trailing vortex structure was examined in detail and ensemble-averaged and instantaneous velocity results obtained to permit understanding of the flow in Eulerian and Lagrangian terms.

The vessel and impeller geometry, instrumentation and measurement techniques are described in the following section. The torque measurements, the flow visualization and the ensemble-averaged and instantaneous velocity results are presented in §3. The measurements are discussed and compared with results of other workers and their implications considered in §4. The paper closes with a summary of the main findings.

2. Flow configuration, instrumentation and procedures

The stirred reactor and impeller geometry and the coordinate system adopted are shown in figure 1. The baffle thickness was 3 mm, and the baffle width was a tenth of the tank diameter. All parts of the vessel, including the baffles, the impeller and the shaft, were made of clear cast acrylic plastic to allow maximum optical access. The cylindrical vessel was placed inside a transparent trough and the gap between the trough and the cylinder filled with water so that the change in refractive index from air ($n_D^{20} = 1.00$) to Perspex ($n_D^{20} = 1.49$) did not occur over the curved surface of the cylinder, but over the flat surface of the trough; the cylinder could be rotated inside the trough with a precision of $\pm 0.125°$, and the whole vessel could be translated in three directions by traversing tables with an accuracy of 0.25 mm.

A heat exchanger with a thermostatic value was incorporated in the bottom of the trough and maintained the water temperature at 20 ± 2 °C. The impeller and shaft

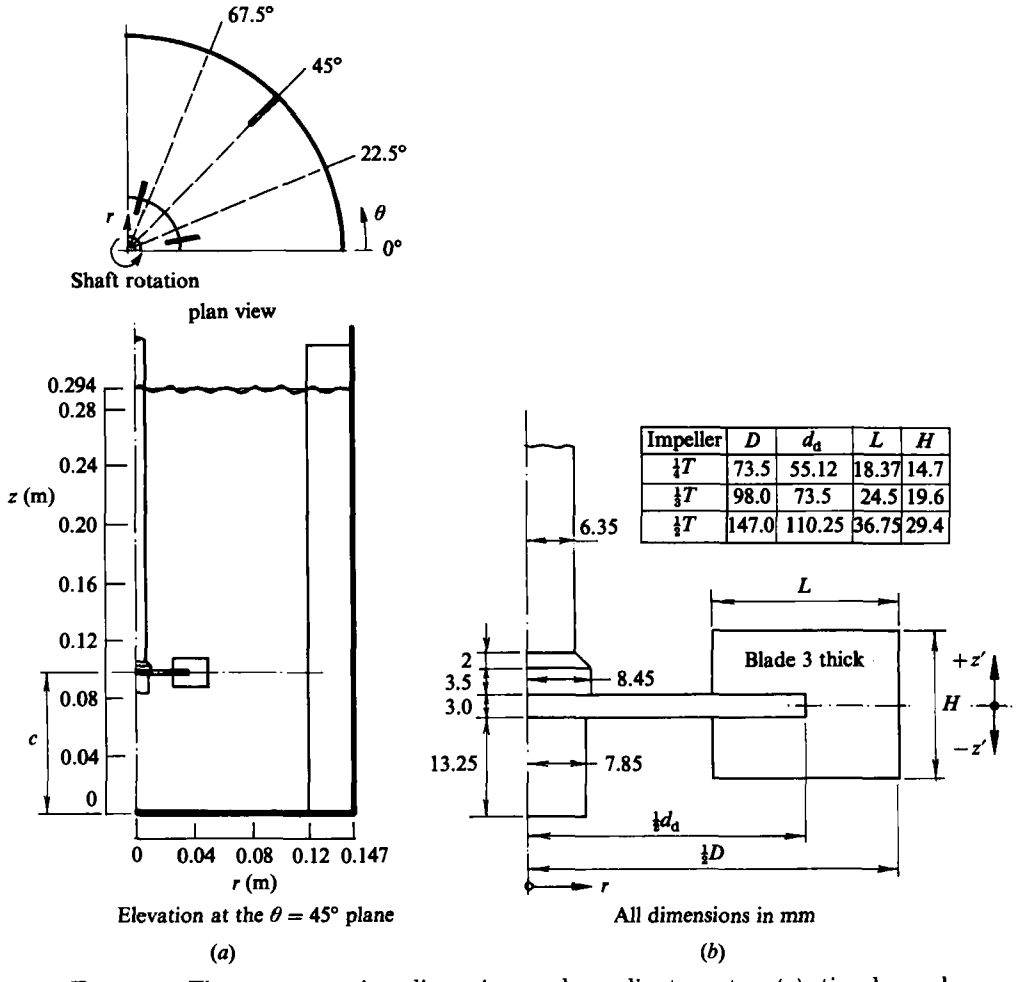

FIGURE 1. Flow concentration, dimensions and coordinate system (*a*) stirred vessel, and (*b*) impeller.

could be removed so that impellers of different diameters (D) and clearances (C) from the bottom of the vessel could be inserted. Water was used as the fluid medium. Three impellers of diameter, in relation to the cylinder diameter ($T = 294$ mm), $D = \frac{1}{4}T$, $\frac{1}{3}T$ and $\frac{1}{2}T$ and three shafts with clearances $C = \frac{1}{4}T$, $\frac{1}{3}T$ and $\frac{1}{2}T$ were used.

The impeller shaft was coupled to an encoder which allowed the synchronization of the velocity measurements with any specified part of each revolution. The encoder provided a train of 999 pulses and a marker pulse in each revolution.

The Reynolds number for the flow is defined as $Re = D^2N\rho/\mu$, where N is the impeller rotational speed and μ and ρ are the dynamic viscosity and the density of the fluid respectively (Uhl & Gray 1966). The blade tip velocity, defined as $V_{tip} = \pi ND$, is employed to characterize the flow at the rotational speed investigated (300 r.p.m.) and for $D = \frac{1}{2}T$, $V_{tip} = 1.54$ m/s and $Re = 48000$. The Power Number, defined as $N_P = P/\rho N^3 D^5$, where P is the power input to the fluid, was measured with an air bearing. Three load cells were used, to allow the accurate measurement of N_P over a range of Reynolds numbers from 10000 to 100000 with a maximum error of 5%.

Half angle of intersection between beams, in air (degrees)	9.15
Fringe separation (line-pair spacing), μm	1.99
Number of fringes in measuring volume (no frequency shift)	84
Intersection volume diameter, calculated at $1/e^2$ intensity, mm	0.167
Intersection volume length, calculated at $1/e^2$ intensity, mm	1.035
Velocity-to-frequency conversion factor, ms^{-1}/MHz	1.99

TABLE 1. Principal characteristics of the laser-Doppler anemometer

Flow visualization was carried out in the stirred reactor to obtain qualitative information on the flow patterns. Planes of the flow seeded with 0.5 mm diameter polystyrene beads were illuminated with a sheet of laser light produced by a cylindrical lens placed in the path of the beam from an Argon-Ion laser operating at 500 mW. Still and cine photography recordings of the flow patterns were made for a variety of flow conditions.

The laser anemometer operated in the fringe, forward-scatter mode and comprised a 15 mW He–Ne laser, a rotating radial diffraction grating and a frequency counter. The principal characteristics of the system are given in Table 1.

The location of the control volume and the change in the beam angle in the vessel due to refraction were calculated by an iterative computer program. As the radius of curvature of the cylinder was large, the effects were small and usually negligible for the measurements made near the impeller. The control volume location with respect to the blade was calculated in r, ϕ, z' coordinates with respect to the impeller, where r is the radius, z' is the elevation from the disk expressed in blade heights H (positive above and negative below the disk) and ϕ the angle behind the leading blade, for the trailing vortex results and in r, z, θ coordinates with respect to the vessel axis for all other results. Positional errors did not exceed 0.05 mm. Measurements in (r, θ)-planes were made with three orientations of the optical axis, 0°, −45° and +22.5°, to yield values of the circumferential (W and $\tilde{w}$) and radial (V and $\tilde{v}$) components as well as $\overline{\tilde{v}\tilde{w}}$, as described by Melling & Whitelaw (1976). The counter could be set to measure all validated Doppler signals or to count only those signals arriving within a prescribed time interval which was set to be 0.003 of a revolution, or 1.08°. The flow was seeded with Diakon particles of less than about 10 μm mean diameter. The data rate was about 1 kHz. In the trailing vortex measurements, the blades travelled a finite arc length relative to the control volume position during the 1.08° interval which varied from 0.7 to 1.3 mm depending on the radius of the measurement location. This introduces a broadening effect on the ensembled mean and turbulent quantities. The maximum errors in the mean velocities are of the order of 1 % of the blade tip velocity rising to 2–3 % in regions where steep gradients are present. Errors in the turbulence fluctuations measured are of the order of 5 % and in the kinetic energy of turbulence of the order of 10 %. A test of the accuracy of the measurements was provided by integrating the velocity profiles measured by averaging over 360° at various planes around the impeller to check the balance of the mass flowing into the impeller region to that flowing out of it: the two results, averaged over four different (r, z)-planes, differed by only 1 %. The axial symmetry of the flow was checked and found to be within the precision of the measurements throughout the vessel.

3. Results

3.1. *Torque measurements and flow visualization*

As expected from Uhl & Gray (1966) the Power Number was found to be nearly invariant with clearance and with rotational speed in the turbulent range ($Re \geqslant 40000$) where $N_P \approx 4.8$. N_P decreased to 4.2 with $D = \frac{1}{4}T$ and increased to 5 with $D = \frac{1}{2}T$.

Sample photographs of the flow visualization carried out to determine the qualitative flow structure are presented in figure 2. They are near-instantaneous recordings of the flow and should not be interpreted as mean flow patterns. The top and bottom ring vortices are almost symmetric about the impeller stream for the $\frac{1}{2}T$ clearance (figure 2*a*) with a near-horizontal impeller stream which is in contrast to that for the $\frac{1}{4}T$ case where the impeller stream is inclined away from the bottom of the vessel. The top ring vortex is more ordered and well defined with the larger clearance and the free surface of the fluid is less flat. The erratic generation and decay of a whirlpool-type of vortex on the free surface was observed for all the configurations and was present even at low rotational speeds, albeit with smaller intensity. This vortex results from the impingement of the impeller stream jet on the baffles; this gives rise to a stable cylindrical eddy and subsequently to two eddies of which one persists as the whirlpool vortex, migrating in the direction of shaft rotation. The effects of this eddy are present in the ensemble-averaged results which were taken over measurement times of 5–10 min. The impeller shaft moved from the symmetry axis during operation by not more than ± 0.25 mm. Recordings of the flow made at rotational speeds of 300 r.p.m. and 100 r.p.m. showed that the flow velocities and the inclination of the impeller stream to the horizontal decreased with rotational speed. The exposure times used in the photographs were 0.5 s and the results represent an average of the fluid motions during 2.5 revolutions of the impeller, so that there were no trailing vortex structures evident. Recordings of the flow visualization were also made in (r, θ)-planes and it was observed that the velocities were smaller than in the (r, z)-plane, and that there is a helical vortex behind the baffle. The visualization also revealed lower velocities for $D = \frac{1}{4}T$ than for $D = \frac{1}{2}T$; for this latter case, the centres of the lower ring vortex are located nearer the axis with the impeller stream more inclined away from the horizontal.

3.2 *Ensemble-averaged mean flow results*

Mean velocity results, obtained by ensemble-averaging over 360°, for the geometry with $D = \frac{1}{3}T$ and $C = \frac{1}{3}T$ are shown in figures 3 and 4 and represent a small sample of the investigation: detailed results are available in a report by Yianneskis, Popiolek & Whitelaw (1984). Figure 3 presents mean velocity vectors $(U^2 + V^2)^{0.5}$ in the (r, z)-plane at $\theta = 0°$. The patterns in the figure consist of two ring vortices (which are similar in all θ planes) and are consistent with the visualization results. The velocities along and near the axis are mainly in the axial direction, with near-uniform profiles approaching the impeller from above and below with magnitudes of about $0.15 V_{\text{tip}}$. At the top and bottom of the vessel, $z = 20$ mm and $z = 260$ mm, radial motion predominates with maximum magnitudes of about 0.2 and $0.1 V_{\text{tip}}$ respectively. The vectors in the $\theta = 45°$ plane were in general larger as the change in geometry induces a faster circulation. The maximum axial velocities recorded in the vortices were of the order of $0.2 V_{\text{tip}}$. The position of the ring vortex centre varied with θ. The mean flowfield around the impeller at $\theta = 0°$ is inclined upwards at the centre by about 4° to the horizontal. The radial velocities in the impeller stream have maxima of

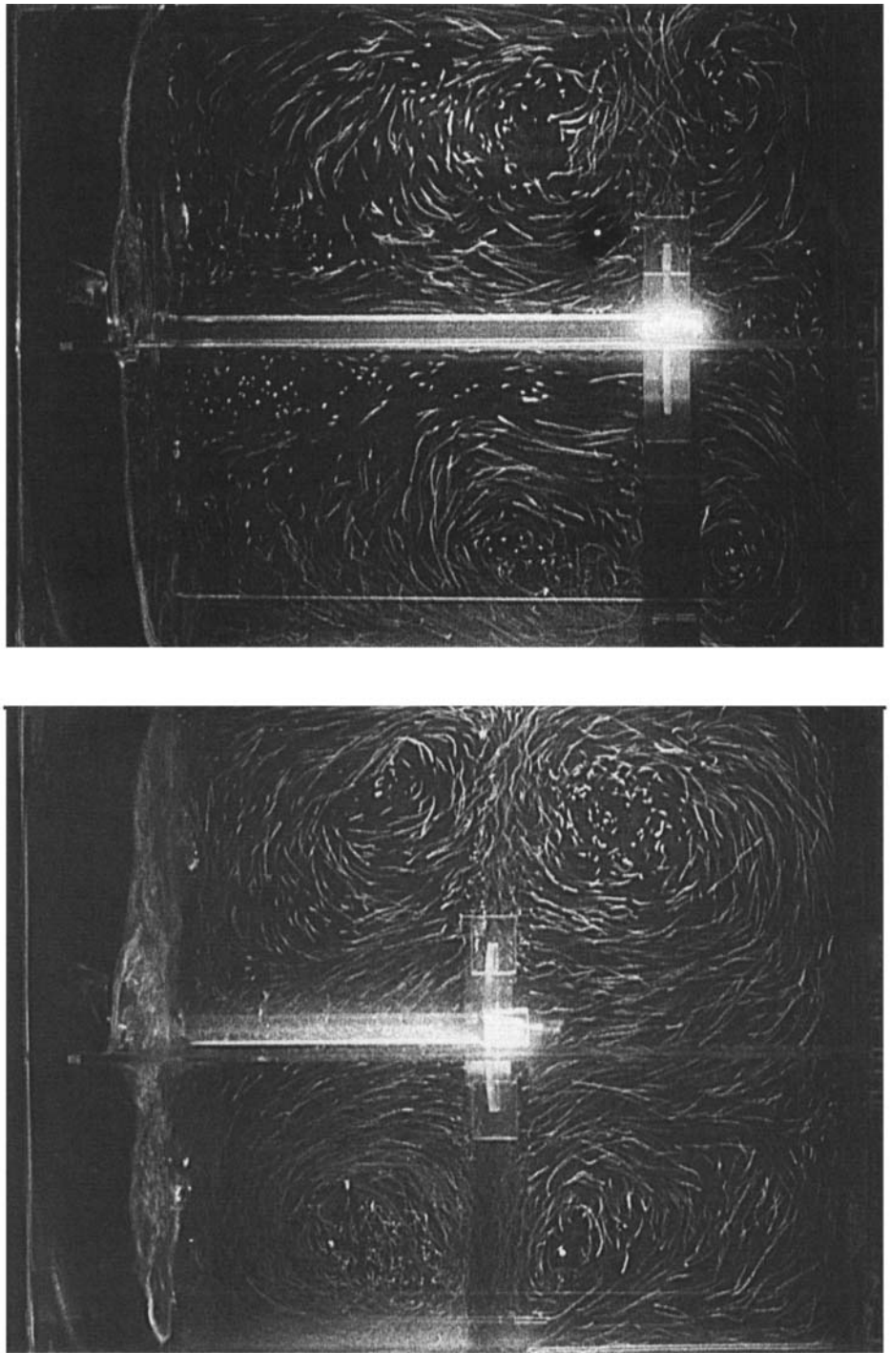

(a) (b)

FIGURE 2. Flow visualization at $\theta = 42.5°$; (a) $D = \frac{1}{3}T$, $C = \frac{1}{2}T$, $N = 300$ r.p.m., and (b) $D = \frac{1}{3}T$, $C = \frac{1}{4}T$, $N = 300$ r.p.m.

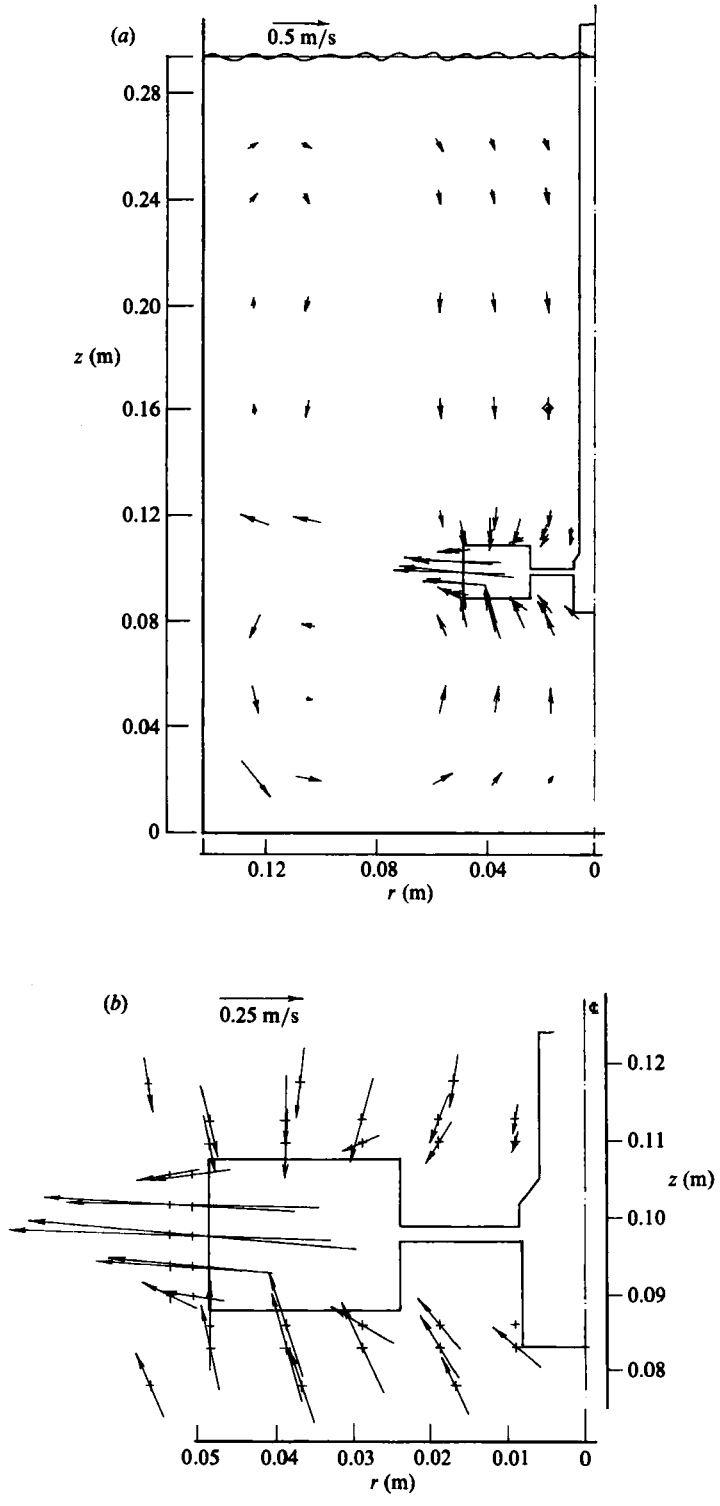

FIGURE 3. Mean velocity vectors in the ($\theta = 0°$) (r, z)-plane. (*a*) Vessel half-section; (*b*) impeller region.

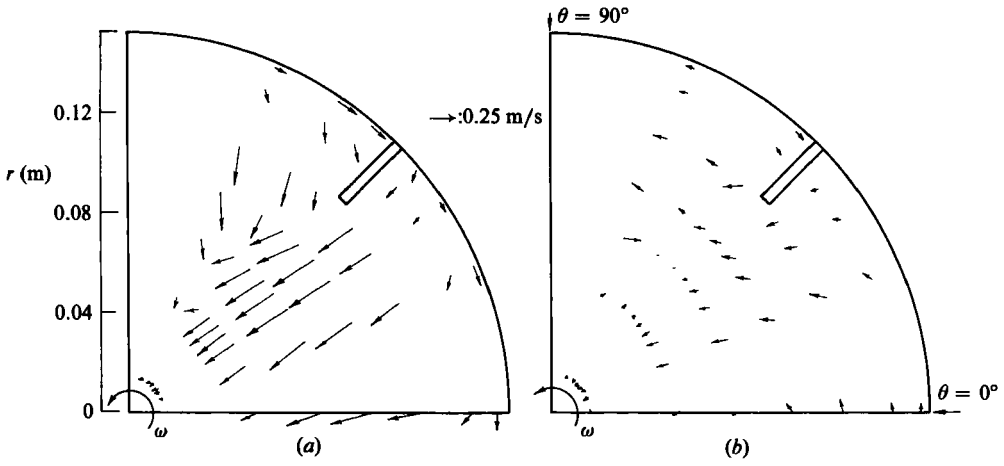

FIGURE 4. Mean velocity vectors in two (r, θ)-planes. (a) $z = 5$ mm, (b) $z = 50$ mm.

$0.7V_{tip}$, and the axial velocities show maxima of around $0.25V_{tip}$ near the middle of the blade both above and below the impeller. Measurements around the impeller were similar in all (r, z)-planes to within 10% of each other.

Mean flow results were also obtained in (r, θ)-planes and those at $z = 5$ mm and $z = 50$ mm are presented in figure 4. The maximum value of W was $0.84V_{tip}$, in the middle of the impeller stream. The profiles of W in the impeller stream were not symmetric about the middle of the blade tip and higher values were measured in the top half. The measurements show that the velocity vectors in (r, θ)-planes i.e. $(V^2 + W^2)^{0.5}$ are small away from the impeller region, and of the order of 0.05–0.1 m/s, and that the flow is of a highly vortical nature. The results indicated that a helical vortex exits behind the baffle. In the rest of the cross-section, the flow is predominantly in the radial direction near the impeller and near the bottom of the vessel, and a part of the ring vortex rotates counter to the impeller rotation and occupies a large region, of about 40 mm in diameter. The velocities at $z = 160$ mm and 200 mm were lower and increased as the free surface was approached at $z = 240$ mm and 260 mm.

The effect of clearance on the impeller stream flow and on the sense of rotation of the lower ring vortex were investigated by making velocity measurements with the $D = \frac{1}{3}T$ impeller for the $\frac{1}{4}T$, $\frac{1}{3}T$ and $\frac{1}{2}T$ clearances for $N = 300$ r.p.m. Profiles of the radial component of the mean velocity at various θ locations showed that the inclination of the impeller stream was about 7.5°, 4° and 2.5° for the $\frac{1}{4}T$, $\frac{1}{3}T$ and $\frac{1}{2}T$ clearances respectively. The maximum velocities were smaller with the largest clearance, about 0.9 of those with the smallest one. The spread of the impeller stream jet tends to increase as the clearance increases. Measurements of W showed that regions of counter-rotating flow and the helical vortices behind the baffles were also present in both the $C = \frac{1}{4}T$ and $C = \frac{1}{2}T$ configurations and that there were large differences in the W distributions measured with different clearances.

3.3 *Trailing vortex mean flow results*

Results obtained by ensemble-averaging over a one-degree interval of rotation in order to resolve the vortex patterns rotating with the blades are presented in this section and the schematic representation of a trailing vortex, figure 5 (a), is provided,

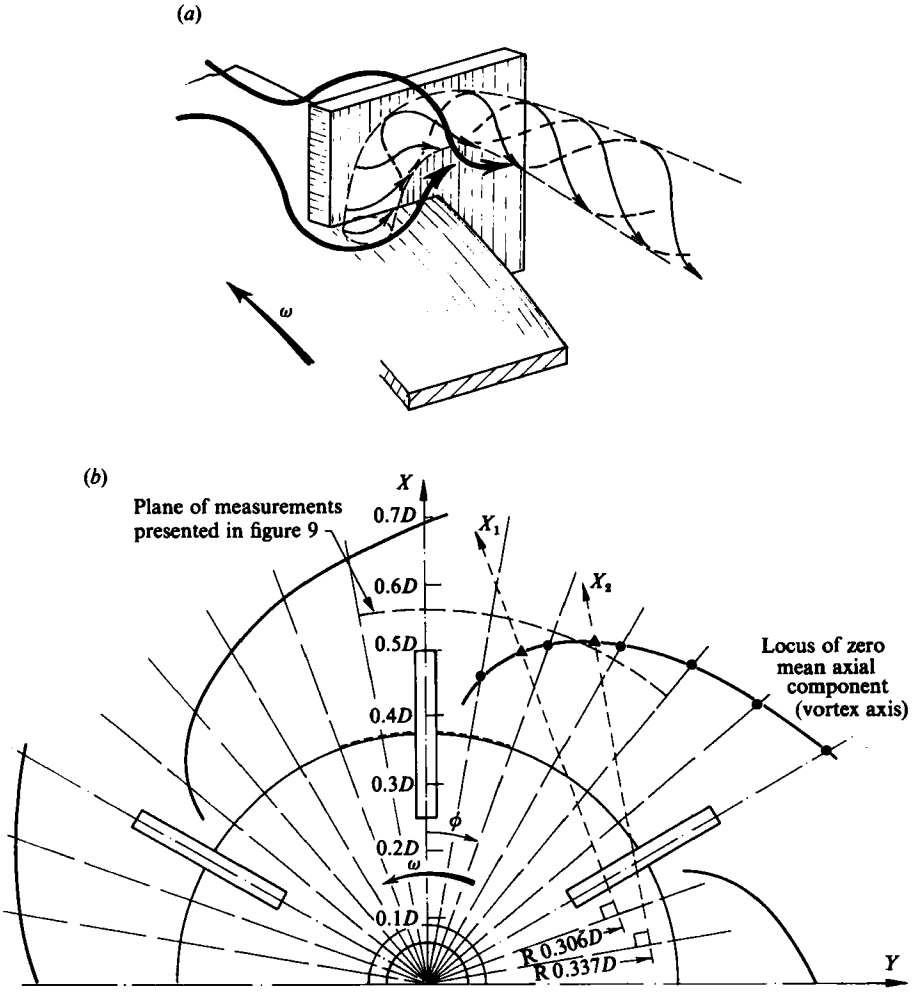

FIGURE 5. (*a*) Schematic representation of a trailing vortex. (*b*) Diagram of the impeller coordinates and of the location of the vortex axis and of the planes of measurement.

to aid understanding of the flow patterns. The location of the centre (or axis) of the vortex can be found by determining the locus where a velocity component perpendicular to the axis is zero. The axial component is more suitable for this measurement, as the displacement of the vortex axis in the z'-direction is small (van't Riet & Smith 1973). The locus of the zero mean axial component was determined by measuring in the z'- and r-directions at six ϕ planes and the result is presented in figure 5(*b*). The radial location of zero axial velocity is shown; the axial location varied by less than 0.5 mm from $z = 0.5H$. The vortex centre is observed to move away from the impeller with increasing distance from the blade, from $r = 0.47D$ at $\phi = 10°$ to $r = 0.7D$ at $\phi = 60°$, i.e. in front of the trailing blade. The radius of this vortex axis can be approximated by the equation $r_a = 30 + 4.93\phi^{\frac{1}{2}}$ (in mm).

The velocity vectors measured in five radial planes (see figure 5*b*) are shown on figure 6. The vectors shown are of magnitudes $(U^2 + V^2)^{0.5}$ The results reveal the expected circulation in the ϕ-planes up to 30° after which it is destroyed by the ring vortex present above the impeller. The velocities reach a maximum of $0.83 V_{tip}$ at

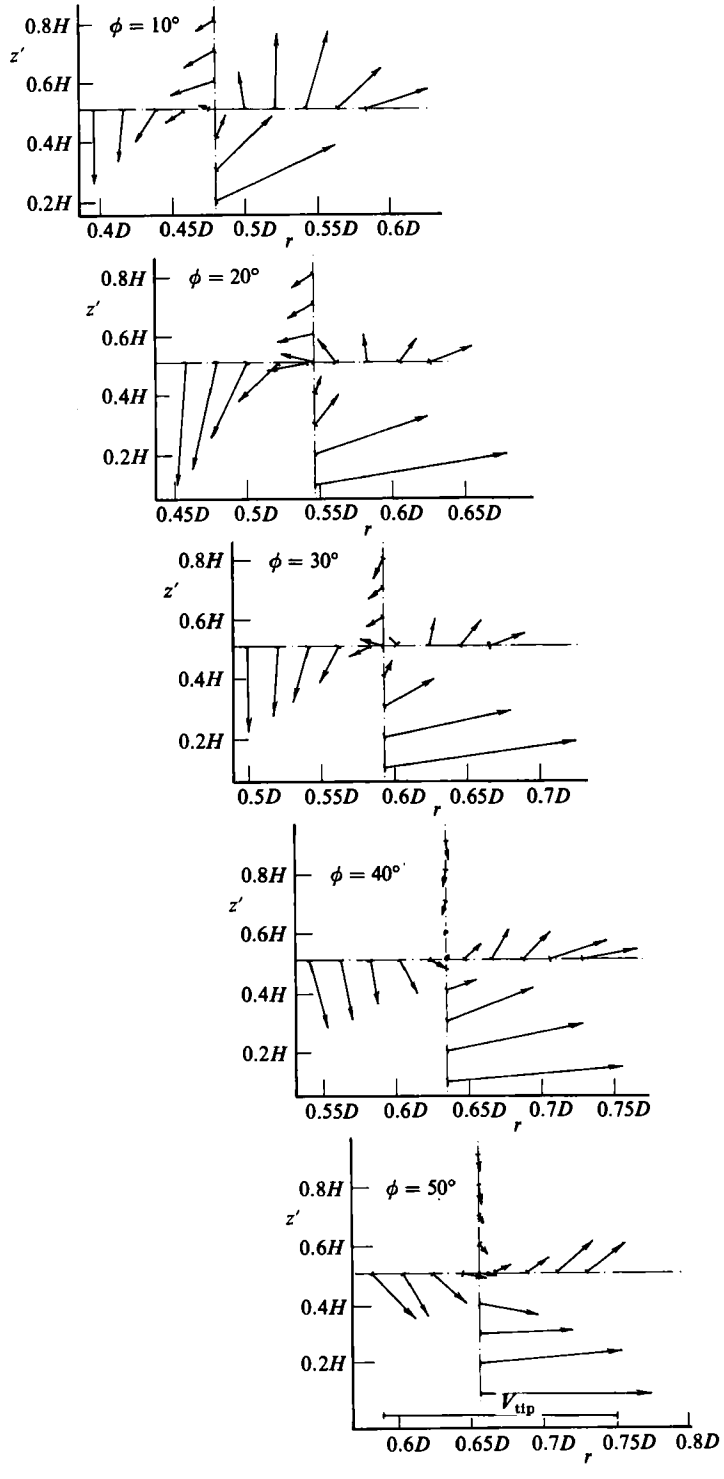

FIGURE 6. Mean velocity vectors in five (r, z')-planes.

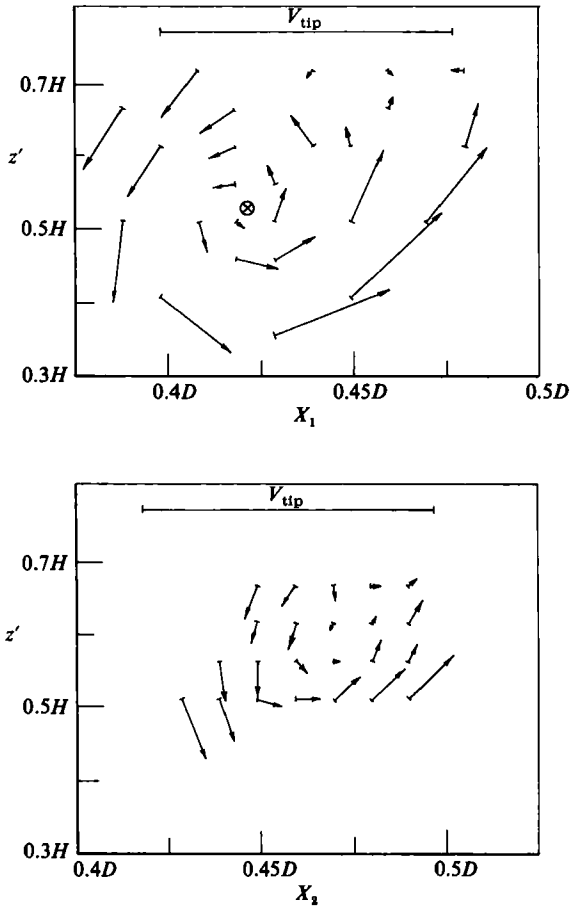

FIGURE 7. Mean velocity vectors in the X_1- and X_2-planes perpendicular to the vortex axis defined in figure 5.

$\phi = 30°$. The results between 10° and 30° suggest that the locus of the vortex centre is slightly different from that measured and shown on figure 5.

In order to determine the vortex structure in planes perpendicular to the vortex axis, measurements were made in the X_1- and X_2-planes defined in figure 5 and are shown in vector form in figure 7. In the X_1-plane, the location of the vortex centre is denoted by the crossed circle symbol and circulation is evident all around this point only up to a radius of 2.5 mm. Velocity magnitudes reach $0.42\,V_{tip}$ in the outer regions, but, within the 5 mm diameter circle in which the vortex is well defined, do not exceed $0.25\,V_{tip}$. The results in the X_2-plane show that the vortex has decayed significantly in magnitude with velocities of less than $0.22\,V_{tip}$ and the circulation is less well defined which suggests that the trailing vortex is influenced by the main ring vortex flow at about 25° behind the leading blade.

The flow behind a blade was measured in detail and figure 8 displays velocities measured in the $\phi = 10°$ (r, z)-plane. The rotational speed of the impeller, ωr at a radius r, was subtracted from the W component measurement to provide an indication of the flow in a Lagrangian frame of reference moving with the impeller. A line denoting the magnitude of the $(-\omega r)$ component of W is also shown. The trailing vortices above and below the impeller disk can be clearly seen in the (r, z')-

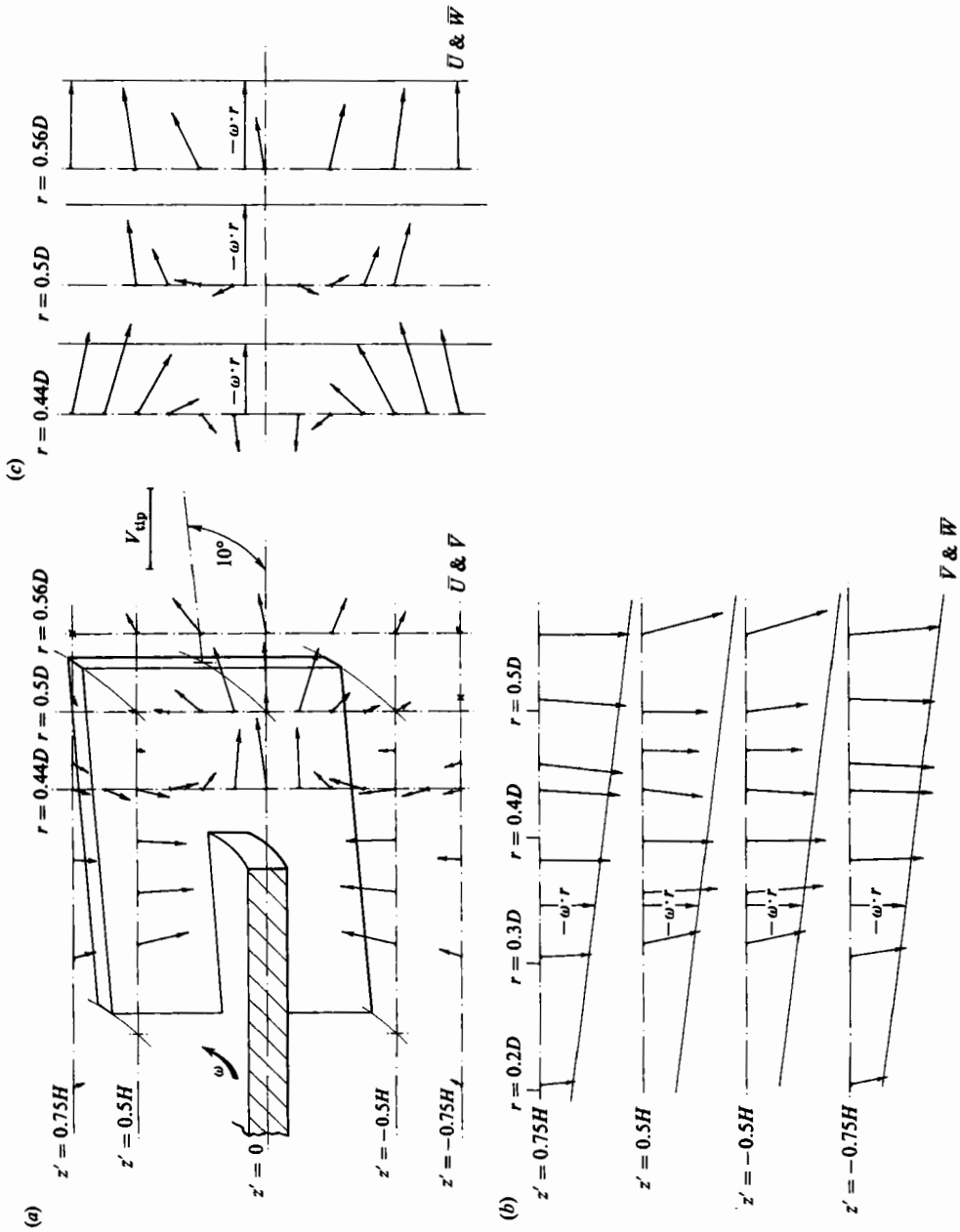

FIGURE 8. Mean velocity vectors in the $\phi = 10°$ (r, z')-plane. (*a*) (r, z')-plane; (*b*) (r, θ)-planes; (*c*) (z', θ)-planes.

and (z', θ)-planes. In the (r, θ)-plane, the velocities are of the order of $-\omega r$, with smaller components near the centre of the vortices (at $z' = \pm 0.5H$).

The velocity distributions in the boundaries of the impeller region for the area between two successive blades were also measured, as they can provide boundary conditions for related calculation methods as well as an understanding of the flow processes. Detailed measurements in a (z', θ)- and various (r, θ)-planes were made to quantify the flow over a blade and to investigate whether a second vortex is generated in front of a blade as has been claimed by Günkel & Weber (1975), but no vortical motion was found there, while the vortex was present behind the blade at $\phi = 5°$ and $10°$ with magnitudes of up to $2\ \omega r$.

3.4. *Ensemble-averaged turbulence results*

Measurements of $\tilde{u}$, $\tilde{v}$ and $\tilde{w}$ (and hence of the kinetic energy of turbulence, $k = 0.5\ (\tilde{u}^2 + \tilde{v}^2 + \tilde{w}^2)$) were obtained for $D = \frac{1}{3}T$ and $C = \frac{1}{3}T$ in the impeller stream and in the lower ring-vortex and of $\tilde{u}$ and $\tilde{v}$ in the upper vortex as 360° ensemble-averages. In the impeller stream measurements were made at 0°, +22.5° and −45° to the local radial direction to allow the determination of the $\overline{\tilde{v}\tilde{w}}$ cross-correlation as well as of $\tilde{v}$ and $\tilde{w}$ fluctuations, see for example Melling & Whitelaw (1976). Since the rate of energy dissipation (ϵ) is important to the mixing processes and also to calculation methods, it was evaluated from measurements with the aid of the effective viscosity hypothesis, assuming $\mu_{\text{eff}} = 0.09\rho k^2/\epsilon$ and axial symmetry in the impeller stream, which was the case to ±5%. The uncertainties associated with this process are inevitably high and the error is of the order of 0.3ϵ.

In the ring vortices the turbulence levels were of the order of 0.1 m/s, reaching higher values in the vicinity of the baffles and in the regions just above and just below the impeller. The maximum recorded value of k was 0.04 m^2/s^2. Elsewhere k was of the order of 0.01 m^2/s^2. The magnitudes of $\tilde{u}$ and $\tilde{v}$ with the $C = \frac{1}{2}T$ and $\frac{1}{4}T$ clearances were similar to those with $C = \frac{1}{3}T$. The $\tilde{w}$ levels below the impeller were 0.1–0.22 m/s for $C = \frac{1}{2}T$ and 0.1–0.18 m/s for $C = \frac{1}{4}T$. The maximum value of k in the impeller stream was approximately 0.4 m^2/s^2, more than an order of magnitude larger than those measured in the lower ring vortex which, in the 22.5° plane, for instance, varied from 0.007 to 0.0318 m^2/s^2. The values of ϵ exhibit a maximum of about 25 m^2/s^3 in the centre of the impeller stream where k is also large and stems from the assumed proportionality between k^2 and ϵ. The $\overline{\tilde{v}\tilde{w}}$ cross-correlation was of the order of 0.1 m^2/s^2. Calculated values of normal and shear-stress production terms showed that they are of similar magnitude and generally smaller than dissipation in the bulk flow. This is consistent with generation in the steeper gradient regions associated with the vicinity of the impeller, and convection and diffusion to the bulk-flow region where the greater proportion of the dissipation occurs. It should be remembered, however, that the contribution of turbulent diffusion to the present flow patterns is generally less than that associated with mean-flow convection and pressure forces. The measured values of turbulence intensity in the impeller stream increase with distance from the impeller tip for all three clearances as the mean velocity decreases in that direction more rapidly than the r.m.s. of the fluctuations. The results indicated that stong anistropy prevails in the fluctuating velocity field. This anisotropy is to be expected since the projected area of the impeller blade in the z- and r-directions is similar and much smaller than that in the θ-direction.

Comparison of the r.m.s. velocities, ensemble-averaged over 1° intervals and over the whole cycle (360° interval) showed that the 1° averages are similar to the 360° ones behind the leading blade and decrease to $\frac{1}{4}$ of the 360° averages where no trailing vortices are present.

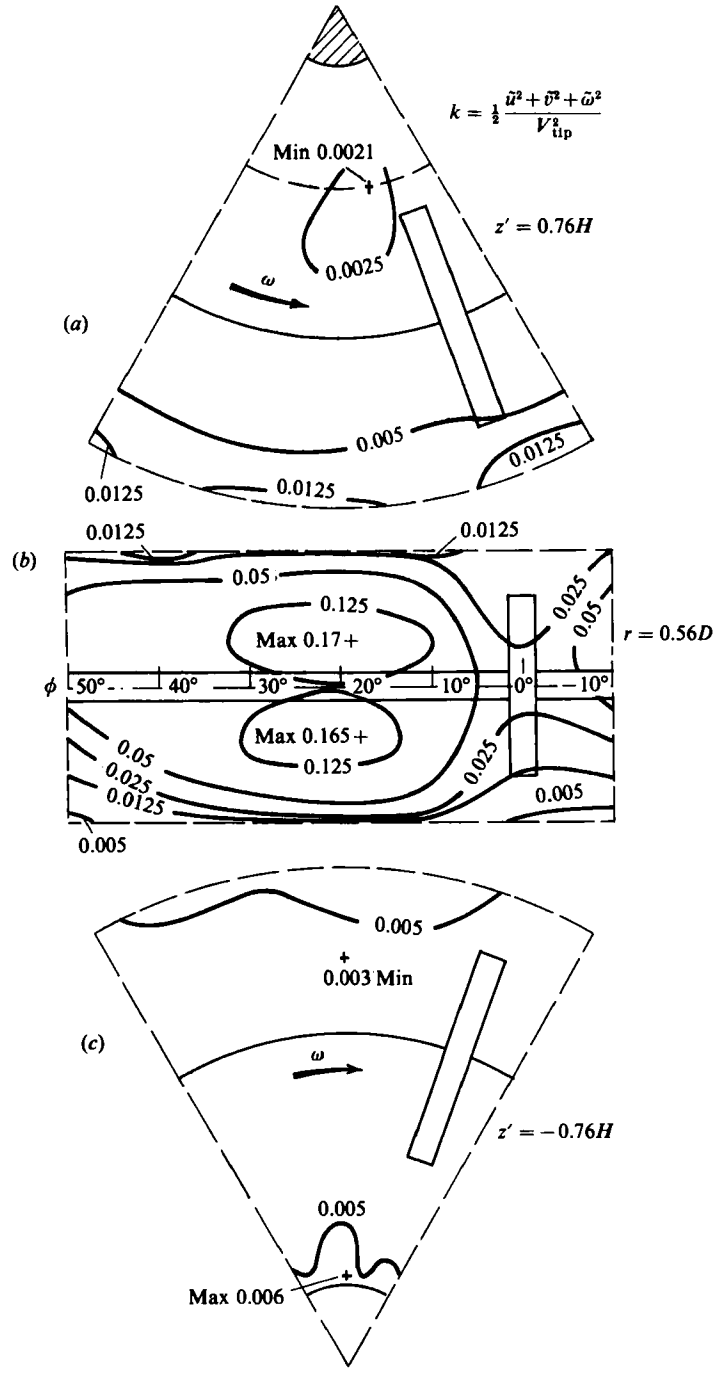

FIGURE 9. Contours of the kinetic energy of turbulence in the planes: (*a*) (r, θ)-plane at $z' = 0.76H$, (*b*) (z', θ)-plane at $r = 0.56D$, (*c*) (r, θ)-plane at $z' = -0.76H$.

In figure 9 contours of the kinetic energy of turbulence, calculated from the 1° ensemble-averages of $\tilde{u}$, $\tilde{v}$ and $\tilde{w}$, are shown. Small values of k exist in the (r, θ)-planes above and below the impeller, while the values at the (z', θ)-plane, are over 50 times larger, and reach a maximum of $0.17\,V_{\text{tip}}^2$. The inclination of the impeller stream noted in the mean flow is evident as higher values of k are displaced towards larger z' values than below the impeller disk. The maximum value of k is located at $\phi = 20°$ behind the blade, and this location correlates well with that of the vortex axis in the ϕ-direction. In front of the blade k values are low, in agreement with the lack of turbulence-generating structures there.

3.5 *Instantaneous velocity results*

As the flow in the vicinity of the impeller is unsteady with cyclic variations, it is important to quantify the cycle-to-cycle variations and to compare the instantaneous with the ensemble-averaged velocity results. Instantaneous velocity traces were recorded in a number of locations and representative results are shown in figure 10. The variation of the axial velocity component at $r = 0.51D$ and $z' = 0.46H$ and $0.51H$ is shown as a function of ϕ (or of time). The trace of figure 10(*a*) extends through three revolutions and the passage of the six blades on each revolution is accompanied by a change in the sign of the U component which signifies the presence of a vortical motion in the z'-direction. The result at $z' = -0.5H$ resembled the inverse of that at $z' = +0.5H$, indicating that there was near symmetry in the instantaneous flow. Similar results were obtained for the V-component. Although six cycles per revolution can be distinguished in most recordings made near the impeller, and periodicity and vortical structures were clearly evident up to $r = 0.7D$, cycle-to-cycle variations are present and are associated with a combination of turbulent fluctuations and the influence of the free surface vortex. Figure 10(*b*) shows six traces of the U-component signal and the ensemble-averaged result over 1° of rotation is reproduced with the individual traces to show the magnitude of the cycle-to-cycle variations. The maximum deviation of instantaneous from ensemble-average velocity is around a factor of two. The ensemble-averaged value for the location of the vortex centre where $U = 0$ is $\phi = 13°$, but varies from 7° to 17° in the instantaneous recordings. In some cycles more than one zero-velocity crossing can be observed and indicates the break-up of the trailing vortex into smaller eddies. The vortical structure is, however, present during most cycles at this radius. Vortex break-up becomes more common with increasing distance from the axis and it can be surmised that the vortices have broken up by $r = 1.0D$.

The results of figure 8 show that the $(U^2 + W^2)^{0.5}$ velocities tend to uniformity from around $r = 0.56D$. In the z'-direction the influence of the vortical structure extends over an even shorter distance and by $z' = \pm 0.75H$, the $(V^2 + W^2)^{0.5}$ velocities are nearly equal to $-\omega r$. This is to be expected in part, as the vortex axis deviates only by about ± 0.5 mm from the horizontal, and as the vortices are convected into the impeller stream. These results are consistent with the final conclusion of the previous paragraph.

4. Discussion

The present results indicate some new features of the flow in stirred vessels, quantify and expand the understanding of previously observed flow phenomena and allow the assessment of current empirical, analytical and numerical models of the flow.

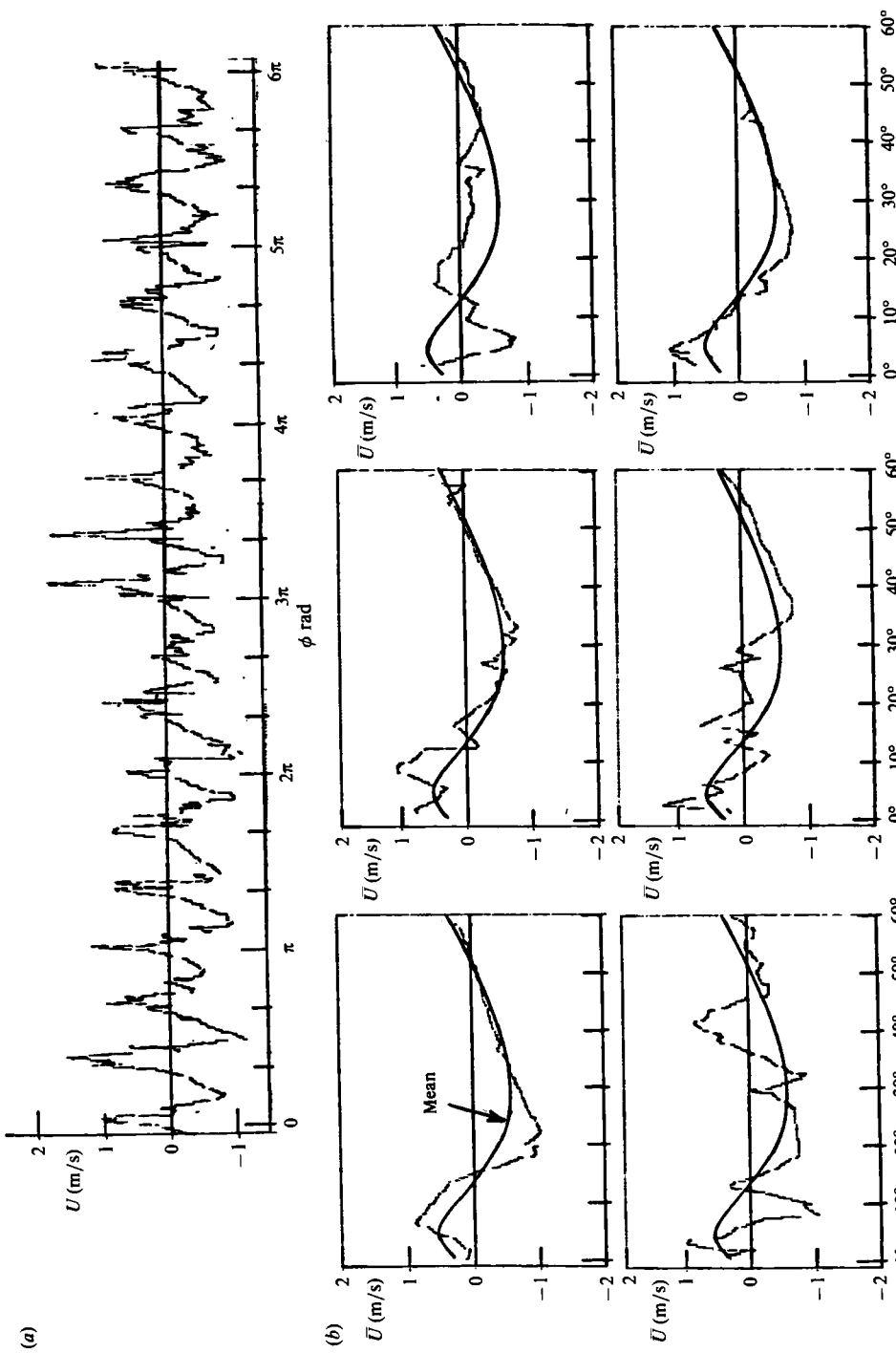

FIGURE 10. (*a*) Instantaneous velocity trace at $r = 0.51D$, $z' = 0.5H$, $\bar{U} = -0.075$ m/s, $\tilde{u} = 0.476$ m/s. (*b*) Cycle-to-cycle variation from the ensemble-averaged axial mean velocity component in the trailing vortices at $r = 0.51D$, $z' = 0.46H$.

The generation of counter-rotating flows in (r, θ)-planes is of particular interest as it has not been quantified before. It is evident that the impeller jet is redirected radially towards the axis by the baffles and that the fluid from the region behind the baffles is drawn into this flow. The pressure gradients existing due to the geometrical and velocity differences are responsible for this counter-rotation. For example, higher velocities are present at $\theta = 45°$ than at $\theta = 67.5°$ where the vessel cross-section is larger and crossflows counterbalance the pressure gradients. Since the circumferential components are small away from the impeller, the crossflows are stronger and result in counter-rotation of the flow.

The flow in (r, z)-planes in the vessel consisted of two ring vortices, except with the $C = \frac{1}{4}T$ and $D = \frac{1}{2}T$ geometry when two additional large vortices were present near the free surface. These vortices occupy the top quarter of the vessel and rotate in the same sense as the lower ring vortex.

The inclination of the impeller stream increases with decreasing clearance and is also a result of the different velocity distributions in the ring vortices and of the associated pressure distribution. For example, the centre of the bottom ring vortex in the $C = \frac{1}{3}T$ configuration is nearer the impeller stream than that of the upper one and the resulting pressure gradient directs the flow upwards. The smaller inclination observed with $C = \frac{1}{2}T$ is also associated with the differences in the two ring vortices, as the free surface affects the shape of the upper vortex in comparison with the lower one.

The present trailing vortices are similar to those of van der Molen & van Maanen (1978) and dominate the flow in the region $0.5D \leqslant r \leqslant 0.75D$ where the maximum circumferential velocities do not exceed $0.5V_{\text{tip}}$. The locus of the present vortex is found nearer the impeller than that observed by van't Riet & Smith (1975) for similar Reynolds numbers but with a larger impeller of 176 mm diameter. This result suggests that the vortex trajectory is dependent upon impeller diameter. The turbulence intensities measured in the present tank are generally higher, partly because van der Molen & van Maanen used a closed top tank without a free surface. In contrast to their findings, turbulence in the impeller stream was found to be anisotropic: $\tilde{u}$ and $\tilde{v}$ values were similar, but $\tilde{w}$ values were different in accordance with the different local gradients generated by an impeller blade which has a larger cross-section in the θ-direction. The rate of decay of the trailing vortex structure indicated by the present results is in agreement with Mujumdar *et al.* (1970) who also observed that the turbulence intensities increased with distance from the impeller. Although the amplitude of the periodicity decreased with distance from the impeller, turbulence levels at two-thirds of the radius were not near-zero as suggested by van der Molen & van Maanen.

The effect of the movement of the impeller shaft on the results was examined, and it was determined that the shaft prescribed the same circular path of 0.25 mm radius during each revolution. Oscillations can be produced in axisymmetric configurations as for example in the electromagnetic stirring of Davidson & Hunt (private communication) but the effect of the slight shaft eccentricity is negligible since the scale of the eccentricity is about one hundredth that of the vortices or of the blades and one thousandth that of the vessel. However, in vessels where the eccentricity is large and/or random in each cycle the results will be strongly affected.

The results suggest dividing the flow into two parts: the impeller stream where periodicity must be accounted for and the instantaneous or the 1° ensemble-averaged results can be used to describe the flow, and the ring-vortex region where 360° averages are appropriate. In both regions the pressure forces are more important than

viscous forces and simple analytical treatments of the flow by separating it into zones, such as that used by Davidson & Hunt for electromagnetically stirring flows, may give good first approximations to the flow patterns.

The empirical values used to characterize the flow are in general agreement with the present data. The impeller discharge coefficient calculated from the present results is 0.785, in agreement with the findings of Revill (1982) who reviewed the existing literature and recommended a value of 0.75 ± 0.15 for a wide range of tank/impeller geometries. However, the measurements show that the usual value of the ratio of the circumferential velocity at the middle of the impeller tip to the tip velocity (the slip factor, 0.7) is underestimated by 15%.

Empirical parameters are also used in numerical modelling and the present results suggest that the specification of uniform conditions for mean and turbulence quantities at the impeller tip is inappropriate, so that, for example, the relationships used by Issa & Gosman (1981) can overestimate the random fluctuations by as much as 200%. On the other hand, the full representation of the trailing vortices is beyond current numerical capabilities and the approximation of their effects by random-plus-periodic fluctuations can be a useful compromise. The continuous-sampling results help to reduce an unsteady (cyclic) flow problem to a steady one by accounting for the presence of the trailing vortices and of the impeller rotation by means of the 'pseudoturbulence' (periodic) fluctuations. The results indicate, however, that numerical resolution of the steep gradients present in the flow will be more important to the solution of the flowfield than the representation of turbulence.

5. Concluding remarks

1. Measurements of the mean velocity components and corresponding turbulence characteristics have been presented for the flow in a stirred tank with an impeller diameter $D = \frac{1}{3}T$ and impeller clearances of $\frac{1}{4}T$, $\frac{1}{3}T$ and $\frac{1}{2}T$. Flow visualization and torque measurements are reported for combinations of these clearances with impellers of $D = \frac{1}{4}T$, $\frac{1}{3}T$ and $\frac{1}{2}T$.

2. The Power Numbers deduced from the torque measurements were around 4.8 and increase slightly with impeller diameter. There was no change in the Power Number with impeller clearance.

3. The flow visualization revealed that variation of the clearance between $\frac{1}{2}T$ and $\frac{1}{4}T$ influenced the inclination of the impeller stream. The impeller diameter affected the shape of the ring vortices and, to a lesser extent than the clearance, the inclination of the impeller stream.

4. Measurements of the radial and circumferential ensemble-averaged velocities below the impeller show a vortical structure in planes perpendicular to the tank axis, with a helical vortex present behind each baffle and large regions of the flow rotating in a sense opposite to that of the impeller. It is evident that the flow was controlled mainly by the balance of pressure and inertia forces.

5. Velocity measurements in the impeller stream with the $\frac{1}{3}T$ impeller at different clearances show that the inclination of the flow from the blades was at an angle of 7.5° away from the disk plane for $C = \frac{1}{4}T$ and this angle was reduced with clearance to 2.5° for $C = \frac{1}{2}T$.

6. The trailing vortex velocity results were obtained as ensemble-averages over intervals of 1° of revolution. A vortical pattern was present at all times up to 20° behind each blade. Cycle-to-cycle variations in the vortical structure were recorded and the instantaneous velocities were different, by up to a factor of two, from the

ensemble-averaged values. The velocities in the vortices were of the order of 0.25 of the blade tip velocity.

7. Measurements of the normal stresses, kinetic energy of turbulence and of the $\overline{vw}$ cross-correlation at the impeller stream for the standard configuration geometry showed that anisotropy prevails in the impeller region with k reaching a maximum of 0.4 m^2/s^2; in the ring vortex, k values are an order of magnitude smaller. Comparison of the results obtained by ensemble-averaging over 1° and 360° of impeller rotation shows that turbulence levels and k can be overestimated up to four times when measurements are made throughout the cycle.

The authors are glad to acknowledge financial support for the present work from Imperial Chemical Industries plc, New Science Group. Z. Popiolek thanks the British Council for their support.

REFERENCES

CUTTER, L. A. 1966 Flow and turbulence in a stirred tank. *AIChE J.* **12**, 35.

GÜNKEL, A. A. & WEBER, M. E 1975 Flow phenomena in stirred tanks. *AIChE J.* **21**, 931.

ISSA, R. I. & GOSMAN, A. D. 1981 The computation of three-dimensional turbulent two-phase flows in mixer vessels. *Proc. Second Intl Conf. on Numerical Methods in Laminar and Turbulent Flow, Venice, 13–16 July 1981.*

MELLING, A. & WHITELAW, J. H. 1976 Turbulent flow in a rectangular duct. *J. Fluid Mech.* **78**, 289.

MUJUMDAR, A. S., HUANG, B., WOLF, D., WEBER, M. E. & DOUGLAS, W. J. M. 1970 Turbulence parameters in a stirred tank. *Can. J. Chem. Engng* **48**, 475.

REED, X. B., PRINCZ, M. & HARTLAND, S. 1977 Laser-Doppler measurements of turbulence in a standard stirred tank. *Second European Conf. on Mixing, Cambridge, 30 March–1 April 1977.*

REVILL, B. K. 1982 Pumping capacity of disc turbine agitators – a literature review. *Fourth European Conf. on Mixing, Noordwijkerhout, Netherlands, 27–29 April 1982.*

UHL, V. W. & GRAY, J. B. 1966 *Mixing-Theory and Practice.* Academic.

VAN DER MOLEN, K. & VAN MAANEN, H. R. E. 1978 Laser-Doppler measurements of the turbulent flow in stirred vessels to establish scaling rules. *Chem. Engng Sci.* **33**, 1161.

VAN'T RIET, K. & SMITH, J. M. 1973 The behaviour of gas–liquid mixtures near Rushton turbine blades. *Chem. Engng Sci.* **28**, 1031.

VAN'T RIET, K. & SMITH, J. M. 1975 The trailing vortex system produced by Rushton turbine agitators. *Chem. Engng Sci.* **30**, 1093.

VAN'T RIET, K., BRUIJN, W. & SMITH, J. M. 1976 Real and pseudo-turbulence in the discharge stream from a Rushton turbine. *Chem. Engng Sci.* **31**, 407.

YIANNESKIS, M., POPIOLEK, Z. & WHITELAW, J. H. 1984 *Imperial College, Mech. Engng Dept Rep.* FS/84/02.